Generalized SAR Processing and Motion Compensation

Evan C. Zaugg
Brigham Young University Microwave Earth Remote Sensing Laboratory
459 Clyde Building, Provo, UT 84602 801-422-4884 zaugg@mers.byu.edu

***Abstract*—Application specific algorithms for processing SAR data have been researched for many years, but a general theory is not well defined. This paper presents a generalized way to look at SAR processing and uses the principles learned to develop an improved motion compensation method. The non-ideal motion of a SAR platform results in degraded image quality, but for known motion, corrections can be made. Traditional motion compensation requires a computationally costly interpolation step to correct translational motion greater than a single range bin. This paper presents an efficient new motion compensation algorithm that corrects this range shift without interpolation. The new method is verified with simulated SAR data and data collected with the NuSAR.**

I. Introduction

IMPROVEMENTS to processing methods for synthetic aperture radar (SAR) data have traditionally been focused on specific algorithms. Research has been conducted and papers published on numerous small tweaks to well established algorithms, but little has been done by way of generalizing the theory of SAR processing. In this paper, the idea of generalized SAR processing theory is presented and applied to a specific application, that of motion compensation.

Motion compensation for airborne synthetic aperture radar (SAR) has always been important for high precision image formation. With high resolution SAR systems now operating on small aircraft and Unmanned Aircraft Systems (UAS's) [1]-[2], which are more susceptible to atmospheric turbulence, motion compensation is receiving renewed attention [3]- [5].

Part of this paper develops a new motion compensation scheme for pulsed SAR systems from the generalized SAR processing point of view. Conventional methods treat motion compensation as a phase correction problem, applying a bulk phase correction to the raw data to correct for a reference range followed by a differential phase correction applied after range compression to account for the range dependence of the motion correction.

This method fails to account for the source of the phase errors, the range shift due to the motion. This is a significant problem when the magnitude of the translational motion is greater than a range bin [6]. Interpolation is sometimes used to address this issue; however, it adds an additional computational burden. This is not acceptable for a high resolution SAR system designed to operate from a UAS and process the data in real-time, such as the NuSAR (developed by the U.S. Naval Research Laboratory, Space Dynamics Laboratory, ARTEMIS Inc., and Brigham Young University).

The generalized SAR processing theory is presented in Section II. The new motion compensation method presented in this paper uses chirp scaling principles to correct the range shift and phase variations caused by translational motion. Section III presents the errors caused by translation motion and the traditional two-step motion compensation algorithm. The new compensation algorithm is developed in Section IV. Section V presents simulation results comparing the proposed algorithm to the traditional method and also presents NuSAR data which is used to verify the new method.

II. Generalized SAR Theory

The three main SAR processing algorithms are the Range-Doppler Algorithm (RDA), the Chirp Scaling Algorithm (CSA), and the Omega-k Algorithm (ω-K). Each algorithm was developed with specific goals in mind and each has its own advantages and dissadvantages. These algorithms are all based on different approximations of the same core theory. Exploration of this general theory makes it easier to understand the conditions for which different approximations are appropriate.

A. The SAR Signal

For our analysis, we only need the phase functions of the SAR signal and we can ignore the initial phase. As in the development presented in [7] we can describe the phase of the demodulated baseband SAR signal as

$$\Phi_0 = -4\pi f_0 R(\eta)/c + \pi K_r(\tau - 2R(\eta)/c)^2 \qquad (1)$$

Where f_0 is the carrier frequency. $R_0(\eta)$ is the range to a given target at slow time η. K_r is the chirp rate and τ is fast time.

The first term describes the azimuth modulation, it consists of the phase left over after demodulation. It is purely a function of the carrier frequency and the changing range to a target. If we were to transmit a single frequency, the second term in Eqn. (1) would be zero and we would still have the same azimuth modulation.

The second term is the transmit chirp delayed by the two-way travel time to the target.

The approximations made in SAR processing algorithms are made to the signal in the wavenumber, or two-dimensional frequency domain. To get an expression for the signal in this domain, we take the range and azimuth FFT's of Eqn. (1).

Using the principle of stationary phase (POSP), we approximate the Fourier transforms. I am not sure what the effect of this approximation is, but we will assume it is negligible.

The range Fourier transform (FT) is performed by adding $-2\pi f_\tau \tau$ to Eqn. (1),

$$\Phi_{0r} = \frac{-4\pi f_0 R(\eta)}{c} + \pi K_r \left[\tau - \frac{2R(\eta)}{c}\right]^2 - 2\pi f_\tau \tau \quad (2)$$

Take the derivative with respect to τ

$$\frac{d\Phi_{0r}}{d\tau} = 2\pi K_r \left[\tau - \frac{2R(\eta)}{c}\right] - 2\pi f_\tau = 0 \quad (3)$$

and solve for τ

$$\tau = \frac{f_\tau}{K_r} + \frac{2R(\eta)}{c} \quad (4)$$

Substitute into Eqn. (2) and simplify to get the signal after the range FFT of the signal.

$$\begin{aligned}\Phi_{1R} &= \frac{-4\pi f_0 R(\eta)}{c} + \frac{\pi f_\tau^2}{K_r} - 2\pi f_\tau \left(\frac{2R(\eta)}{c} + \frac{f_\tau}{K_r}\right) \\ &= \frac{-4\pi f_0 R(\eta)}{c} - \frac{\pi f_\tau^2}{K_r} + \frac{-4\pi f_\tau R(\eta)}{c} \\ &= \frac{-4\pi (f_0 + f_\tau) R(\eta)}{c} - \frac{\pi f_\tau^2}{K_r} \end{aligned} \quad (5)$$

where f_τ is range frequency.

We now expand the range to the target $R(\eta)$

$$R(\eta) = \sqrt{R_0^2 + v^2\eta^2} \quad (6)$$

where R_0 is the range of closest approach, and v is the velocity.

$$\Phi_{1R} = \frac{-4\pi (f_0 + f_\tau)\sqrt{R_0^2 + v^2\eta^2}}{c} - \frac{\pi f_\tau^2}{K_r} \quad (7)$$

Again using the POSP, we subtract $2\pi f_\eta \eta$ and take the derivative with respect to η

$$\Phi_{1Ra} = \frac{-4\pi (f_0 + f_\tau)\sqrt{R_0^2 + v^2\eta^2}}{c} - \frac{\pi f_\tau^2}{K_r} - 2\pi f_\eta \eta \quad (8)$$

$$\frac{d\Phi_{1Ra}}{d\eta} = \frac{-4\pi f_0 v^2 \eta}{c\sqrt{R_0^2 + v^2\eta^2}} + \frac{-4\pi f_\tau v^2 \eta}{c\sqrt{R_0^2 + v^2\eta^2}} - 2\pi f_\eta = 0 \quad (9)$$

solve for η

$$\begin{aligned}\eta &= -\frac{c f_\eta R_0}{v\sqrt{-f_\eta^2 c^2 + 4v^2 f_0^2 + 8v^2 f_0 f_\tau + 4v^2 f_\tau^2}} \\ &= -\frac{c f_\eta R_0}{2(f_0 + f_\tau)v^2\sqrt{1 - \frac{c^2 f_\eta^2}{4v^2(f_0+f_\tau)^2}}} \end{aligned} \quad (10)$$

Substitute into Eqn. (8) and simplify with some algebraic manipulation

$$\begin{aligned}\Phi_{1RA} &= -\frac{4\pi(f_0 + f_\tau)\sqrt{R_0^2 + \frac{v^2 c^2 R_0^2 f_\eta^2}{(f_0+f_\tau)^2 v^4\left(4 - \frac{f_\eta^2 c^2}{v^2(f_0+f_\tau)^2}\right)}}}{c} \\ &+ \frac{\pi c R_0 f_\eta^2}{(f_0 + f_\tau)v^2\sqrt{1 - \frac{c^2 f_\eta^2}{4v^2(f_0+f_\tau)^2}}} - \frac{\pi f_\tau^2}{K_r} \\ &= -\frac{4\pi R_0 (f_0 + f_\tau)}{c\sqrt{1 - \frac{c^2 f_\eta^2}{4v^2(f_0+f_\tau)^2}}} \\ &+ \frac{\pi c R_0 f_\eta^2}{(f_0 + f_\tau)v^2\sqrt{1 - \frac{c^2 f_\eta^2}{4v^2(f_0+f_\tau)^2}}} - \frac{\pi f_\tau^2}{K_r} \\ &= -\frac{4\pi R_0 (f_0 + f_\tau)}{c}\sqrt{1 - \frac{c^2 f_\eta^2}{4v^2(f_0 + f_\tau)^2}} - \frac{\pi f_\tau^2}{K_r} \\ &= -\frac{4\pi R_0 f_0}{c}\sqrt{D^2(f_\eta) + \frac{2f_\tau}{f_0} + \frac{f_\tau^2}{f_0^2}} - \frac{\pi f_\tau^2}{K_r} \end{aligned} \quad (11)$$

where

$$D(f_\eta) = \sqrt{1 - \frac{c^2 f_\eta^2}{4v^2 f_0^2}} \quad (12)$$

and f_η is azimuth frequency.

Eqn. (11) is the phase of the SAR signal in the wavenumber domain. For a target at a given range R_{ref}, the target can be ideally focused (the best we can do with the POSP approximation of the FFT) with the reference function multiply

$$H_{RFM} = \frac{4\pi R_{ref} f_0}{c}\sqrt{D^2(f_\eta) + \frac{2f_\tau}{f_0} + \frac{f_\tau^2}{f_0^2}} + \frac{\pi f_\tau^2}{K_r} \quad (13)$$

This works regardless of squint, beamwidth, and chirp bandwidth.

B. SAR Approximations

The Omega-K algorithm uses the exact representation of Eqns. (11 and 13) for a reference range. Then an interpolation is done to correct for all other ranges. This makes the ω-K algorithm a good choice for systems with low-frequency, a large beamwidth, and a large bandwidth. This precision comes at the cost of high complexity and high processing time.

Other algorithms make a Taylor series approximation of Eqn. (11). The square root term can be expanded as

$$\begin{aligned}\Upsilon(f_\tau) &= \sqrt{D^2(f_\eta) + \frac{2f_\tau}{f_0} + \frac{f_\tau^2}{f_0^2}} \\ &\approx \Upsilon(0) + \frac{\Upsilon'(0)}{1!}f_\tau + \frac{\Upsilon''(0)}{2!}f_\tau^2 + \frac{\Upsilon'''(0)}{3!}f_\tau^3 \ldots \end{aligned} \quad (14)$$

RDA keeps only the 0th order term

$$\Phi_{RDA} \approx -\frac{4\pi R_0 f_0}{c} \cdot [D(f_\eta)] - \frac{\pi f_\tau^2}{K_r} \quad (15)$$

which makes the algorithm relatively simple. The first term of Eqn. (15) is the azimuth modulation, corrected in the range-Doppler domain during "azimuth compression." The

second term is the chirp modulation corrected in the "range compression step." The range-cell migration (RCM) correction is an interpolation that makes up for the neglected RCM term and the secondary range compression compensates for higher order terms.

The CSA keeps up to the second order terms

$$\Phi_{CSA} \approx -\frac{\pi f_\tau^2}{K_r} - \frac{4\pi R_0 f_0}{c} \cdot \left[D(f_\eta) + \frac{f_\tau}{f_0 D(f_\eta)} + \frac{D^2(f_\eta)-1}{2f_0^2 D^3(f_\eta)} f_\tau^2\right] \quad (16)$$

In the square brackets, the first term is the azimuth modulation, the second term is the range-cell migration, and the third term is "cross-coupling" between the range and azimuth frequencies.

Further expanding Eqn. (14) yields

$$\Upsilon(f_\tau) \approx D(f_\eta) + \frac{f_\tau}{f_0 D(f_\eta)} + \frac{D^2(f_\eta)-1}{2f_0^2 D^3(f_\eta)} f_\tau^2 - \frac{D^2(f_\eta)-1}{2f_0^3 D^5(f_\eta)} f_\tau^3 - \frac{5-6D(f_\eta)^2+D(f_\eta)^4}{8f_0^4 D^7(f_\eta)} f_\tau^4 \ldots \quad (17)$$

From this equation we can explore how the approximations effect the signal at different frequencies and bandwidths. Simulated data is used to illustrate each point. In the simulation, there is a single target at a known range. Using Eqn. (13) the target can be "perfectly" focused. This perfect example is compared to processing the same data with approximations of Eqn. (13) of different order expansions. With lower frequencies, higher bandwidths, and higher beamwidths, the higher order terms become more important.

Approximations work well for high frequency SAR's. When f_0 is big, $D(f_\eta) \approx 1$. At Ka-band, for example, higher order terms in Eqn. (17) are very nearly zero, thus only low order approximations are needed (see Figure 1).

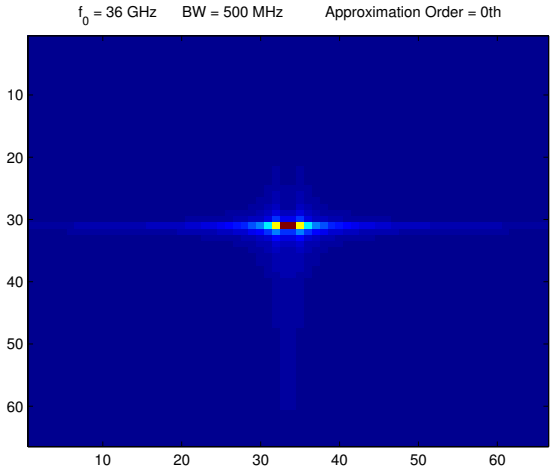

Fig. 1. At Ka-band, a high bandwidth signal can be properly focused using a low order approximation.

Dropping the center frequency to C-band (see Figure 2), the same order approximation is not sufficient for proper focusing, but the second order approximation of the CSA would work well.

At 550 MHz, the second order approximation does not perform well (see Figure 3). To get good focusing, terms up to the fifth order must be accounted for (see Figure 4).

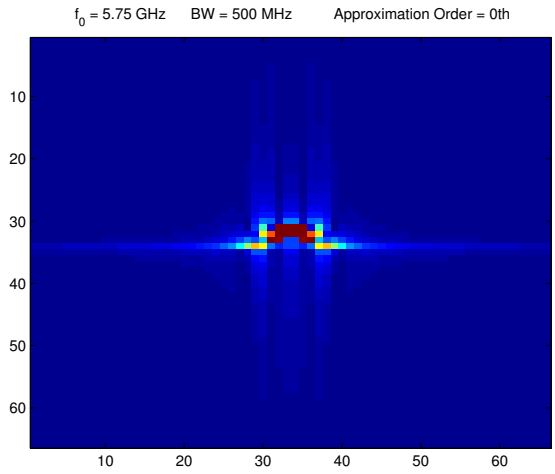

Fig. 2. At C-band, the high bandwidth signal is not properly focused without taking into account some higher order terms.

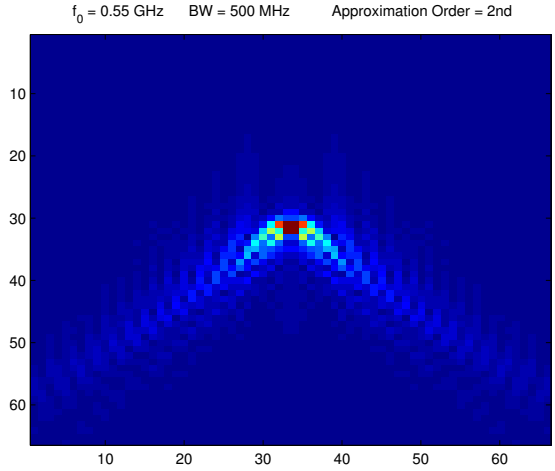

Fig. 3. For lower frequencies, the standard second order approximation is not sufficient for proper focusing.

The interaction between frequency, beamwidth, and bandwidth is shown in the plots of Figure 5. Quantifying this relationship and specifying criteria for determining the number of terms required for focusing a given set of SAR data are the next steps to be taken in this research.

III. Translational Motion Errors

Basic SAR processing assumes that the platform moves in a straight line. In any actual data collection this is not the case, as the platform experiences a variety of deviations from the ideal path. These deviations introduce errors in the collected data which degrade the SAR image.

Translational motion causes platform displacement from the nominal, ideal path. This results in the target scene changing in range during data collection. This range shift also causes inconsistencies in the target phase history [8]. A target at range R is measured at range $R+\Delta R$ which introduces a phase shift of

$$\phi_{\mathrm{m}} = \frac{-2\Delta R \cdot 2\pi}{\lambda} \quad (18)$$

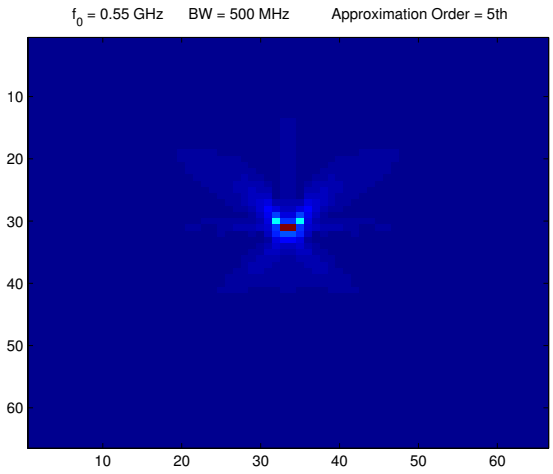

Fig. 4. The lower the frequency, the more terms from the expansion in Eqn. (17) are required.

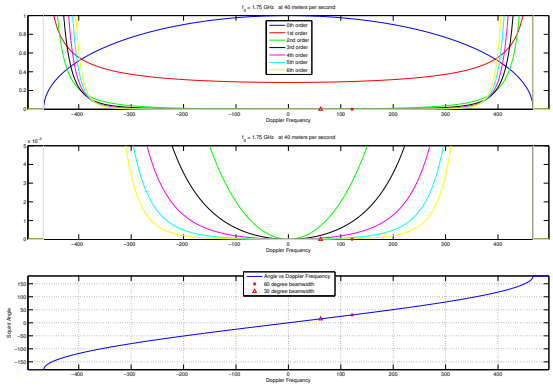

Fig. 5. The top two plots show the different order terms from Eqn. (17 with the relative magnitudes. The third plot shows beamwidth angles corresponding to the Doppler frequencies. Beamwidths that could be used in practice are plotted on all three plots to emphasize how the beamwidth impacts the number of terms required for proper focusing.

in the data. Fortunately, if the motion in known (usually from an on-board INS/GPS sensor), then the motion errors can be corrected.

The common method for compensating for the non-ideal motion has been developed for specific algorithms (RDA and CSA) and involves two steps. First, the corrections are calculated for a reference range, R_{ref}, usually in the center of the swath. The phase correction

$$H_{\text{mc1}} = \exp\left(j\frac{4\pi\Delta R_{\text{ref}}}{\lambda}\right) \tag{19}$$

is applied to the raw data.

The SAR data is range compressed. A second order correction is applied to each range according to the differential correction from the reference range. For each R, ΔR is calculated and the correction is formed,

$$H_{\text{mc2}} = \exp\left(j\frac{4\pi\left(\Delta R - \Delta R_{\text{ref}}\right)}{\lambda}\right). \tag{20}$$

At this point the motion-induced range shift can be removed through a computationally taxing interpolation. This method is commonly used in range-Doppler (RDA) processing and chirp-scaling (CSA) for SAR image generation.

IV. New Motion Compensation

To formulate a new motion compensation scheme we start with the exponential terms of the demodulated SAR signal, as defined in Eqn. (1),

$$s_0(\tau,\eta) = e^{(-j4\pi f_0 R(\eta)/c)} \cdot e^{\left(j\pi K_r(\tau - 2R(\eta)/c)^2\right)} \tag{21}$$

where τ is fast (range) time, η is slow (along-track) time, f_0 is the center frequency, $R(\eta)$ is the range to target, c is the speed of light, and K_r is the chirp rate.

Looking at motion from a general point of view we can apply the principles of Section II to the motion compensation problem. With translational motion, the range $R(\eta)$ becomes $R(\eta)+\Delta R(\eta)$. We split the motion term into range-dependent, $\Delta R_{\text{diff}}(\eta)$, and range-independent, $\Delta R_{\text{ref}}(\eta)$, terms,

$$\Delta R(\eta) = \Delta R_{\text{ref}}(\eta) + \Delta R_{\text{diff}}(\eta), \tag{22}$$

which changes the demodulated signal, Eq. (21), to

$$\begin{aligned} s_m(\tau,\eta) = \quad & e^{\left(-j4\pi f_0 \frac{R(\eta)+\Delta R_{\text{ref}}(\eta)+\Delta R_{\text{diff}}(\eta)}{c}\right)} \\ & \cdot e^{\left(j\pi K_r\left(\tau - 2\frac{R(\eta)+\Delta R_{\text{ref}}(\eta)+\Delta R_{\text{diff}}(\eta)}{c}\right)^2\right)} \end{aligned} \tag{23}$$

which expands into

$$\begin{aligned} s_m(\tau,\eta) = \quad & e^{(-j4\pi f_0 R(\eta)/c)} \cdot e^{\left(j\pi K_r(\tau - 2R(\eta)/c)^2\right)} \\ & \cdot e^{\left(j4\pi K_r \frac{\Delta R_{\text{ref}}(\eta)^2}{c^2}\right)} \cdot e^{\left(-j4\pi f_0 \frac{\Delta R_{\text{ref}}(\eta)}{c}\right)} \\ & \cdot e^{(-j4\pi K_r \tau \Delta R_{\text{ref}}(\eta)/c)} \\ & \cdot e^{\left(j8\pi K_r \Delta R_{\text{ref}}(\eta)(\Delta R_{\text{diff}}(\eta)+R(\eta))/c^2\right)} \\ & \cdot e^{\left(j\frac{4\pi K_r \Delta R_{\text{diff}}(\eta)^2}{c^2}\right)} \cdot e^{\left(j\frac{8\pi K_r R(\eta)\Delta R_{\text{diff}}(\eta)}{c^2}\right)} \\ & \cdot e^{\left(-j4\pi f_0 \frac{\Delta R_{\text{diff}}(\eta)}{c}\right)} \cdot e^{\left(-j4\pi K_r \tau \frac{\Delta R_{\text{diff}}(\eta)}{c}\right)} \end{aligned} \tag{24}$$

where the first two terms are the desired signal, Eq. (21), the next three terms are the range-independent errors, and the last five terms are the range-dependent errors.

The proposed method also follows a two step scheme but eliminates the need for interpolation. The first correction is applied to the raw data.

$$M_1(\tau,\eta) = e^{\left(\frac{-j4\pi\Delta R_{\text{ref}}(\eta)\left(-f_0 c - K_r \tau c + K_r \Delta R_{\text{ref}}(\eta)\right)}{c^2}\right)}. \tag{25}$$

It cancels the range-independent errors and shifts the targets in range.

The data is then range compressed with a common algorithm (RDA or CSA). We simplify the next step by assuming that the range-dependent errors do not change during range compression. This introduces additional phase errors that we ignore, with future efforts planned to track the phase errors through the processing steps and fully integrate it into the general theory. The second motion correction is applied to the

range compressed data, cancelling the range-dependent error terms,

$$M_2(R,\eta) = e^{\left(-j8\pi K_r \Delta R_{\mathrm{ref}}(\eta)(\Delta R_{\mathrm{diff}}(\eta)+R(\eta))/c^2\right)} \cdot e^{\left(-j\frac{4\pi K_r \Delta R_{\mathrm{diff}}(\eta)^2}{c^2} - j\frac{8\pi K_r R(\eta)\Delta R_{\mathrm{diff}}(\eta)}{c^2}\right)} \cdot e^{\left(j4\pi f_0 \frac{\Delta R_{\mathrm{diff}}(\eta)}{c}\right)} \cdot e^{\left(j4\pi K_r \tau \frac{\Delta R_{\mathrm{diff}}(\eta)}{c}\right)} \quad (26)$$

where $\tau = 2R/c$.

V. Results

SAR data, simulated with parameters matching the X-Band NuSAR described below, is used to verify the proposed motion compensation algorithm. In Fig. 6 a single point target is shown to have better range and azimuth resolution after applying the proposed motion compensation algorithm. Fig. 7 shows an array of point targets with the same motion as in Fig. 6. The results of the proposed motion compensation algorithm are dramatically better for translational motion of larger magnitude, as is demonstrated in Fig. 8.

The NuSAR is designed for UAS flight operating at L-Band or X-Band a 500 MHz bandwidth giving a 30 cm resolution. Fig. 9 shows an area imaged with the NuSAR and processed with the CSA. The application of the standard and proposed motion compensation algorithms is shown. Unfortunately the motion compensation in this example is limited by low quality motion data, nevertheless the image quality is enhanced by using the motion compensation algorithms. The improvements are most noticeable in the increased sharpness of the fine details. The processing time is virtually identical for the two motion compensation methods.

VI. Conclusion

The idea of a general SAR processing theory has been presented, showing how the common processing algorithms are approximations. This idea has been used to develop an improved motion compensation algorithm for pulsed SAR. The results show that it properly corrects the effects of non-ideal motion while offering some advantages. The proposed method can be implemented in place of the traditional method to improve processing efficiency and accuracy. Further efforts in exploring this general theory may lead to further advances in SAR processing.

References

[1] P.A. Rosen, S. Hensley, K. Wheeler, G. Sadowy, T. Miller, S. Shaffer, R. Muellerschoen, C. Jones, H. Zebker, and S. Madsen, "UAVSAR: A New NASA Airborne SAR System for Science and Technology Research", in *2006 IEEE Conference on Radar*, pp. 24-27, April 2006.

[2] E.C. Zaugg, D.L. Hudson, and D.G. Long, "The BYU μSAR: A Small, Student-Built SAR for UAV Operation", in *Proc. Int. Geosci. Rem. Sen. Symp.*, Denver Colorado, pp.411-414, Aug. 2006.

[3] S.N. Madsen, "Motion Compensation for Ultra Wide Band SAR", in *Proc. Int. Geosci. Rem. Sen. Symp.*, Sydney, NSW, pp.1436-1438, July 2001 .

[4] A. Meta, J.F.M. Lorga, J.J.M. de Wit, and P. Hoogeboom, "Motion compensation for a high resolution Ka-band airborne FM-CW SAR", in *European Radar Conference, EURAD 2005*, pp. 391-394, Oct. 2005.

[5] E.C. Zaugg, and D.G. Long, "Full Motion Compensation for LFM-CW Synthetic Aperture Radar", in *Proc. Int. Geosci. Rem. Sen. Symp.*, Barcelona, Spain, pp. 5198-5201, Jul. 2007.

[6] A. Moreira, and Y. Huang, "Airborne SAR processing of highly squinted data using a chirp scaling approach with integrated motion compensation", in *IEEE Trans. Geosci. Remote Sensing*, vol. 32, pp. 1029-1040, Sept. 1994.

[7] I.G. Cumming, and F.H. Wong, *Digital Processing of Synthetic Aperture Radar Data*, Artech House, 2005.

[8] G. Franceschetti and R. Lanari, *Synthetic Aperture Radar Processing*, CRC Press, New York, 1999.

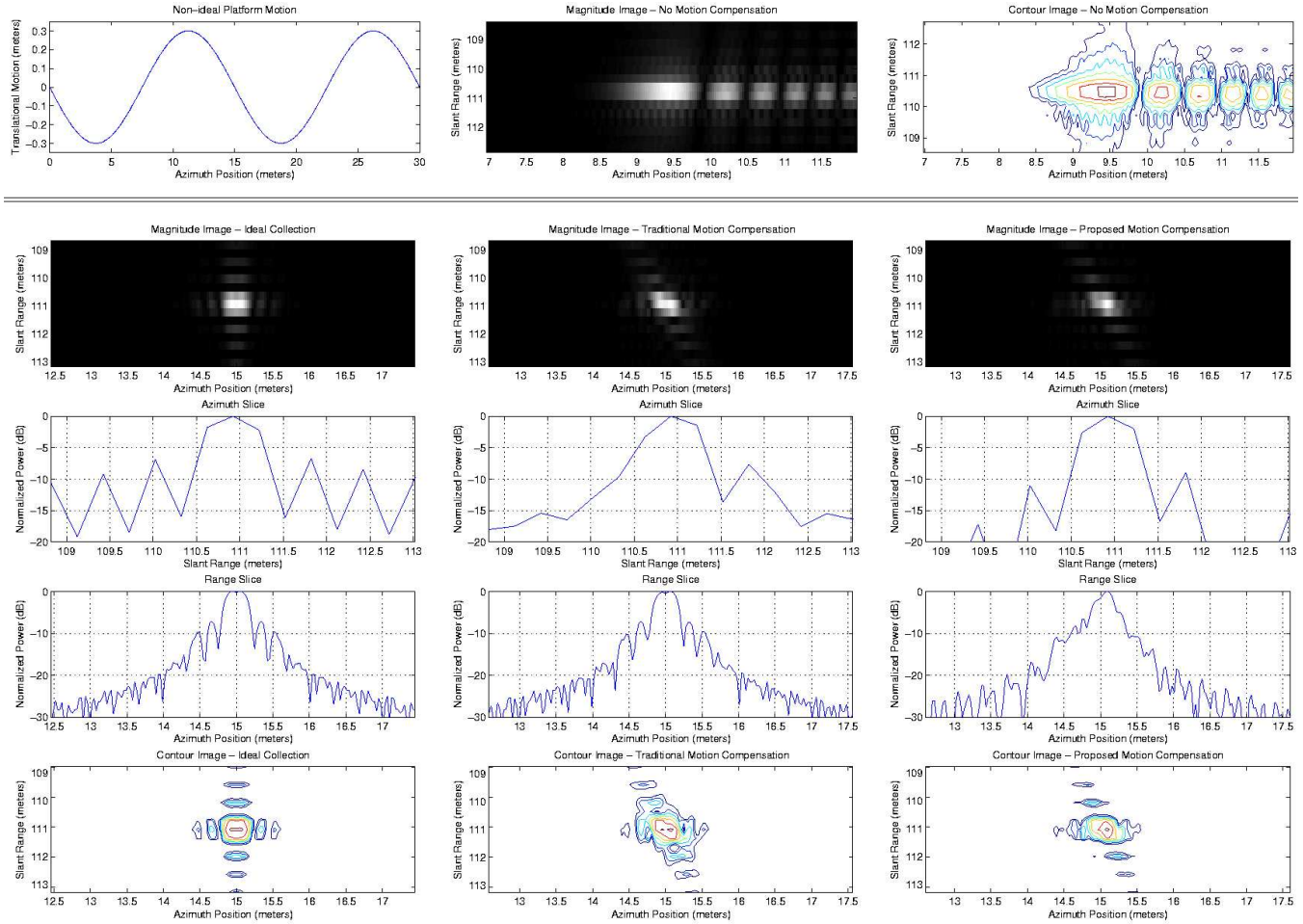

Fig. 6. Simulated SAR data of a single point target imaged with sinusoidal translational motion. The first column shows an ideal collection without non-ideal motion, the top row shows the translational motion and the image without compensation, the middle column shows the results of traditional motion compensation, and the rightmost column shows the proposed motion compensation.

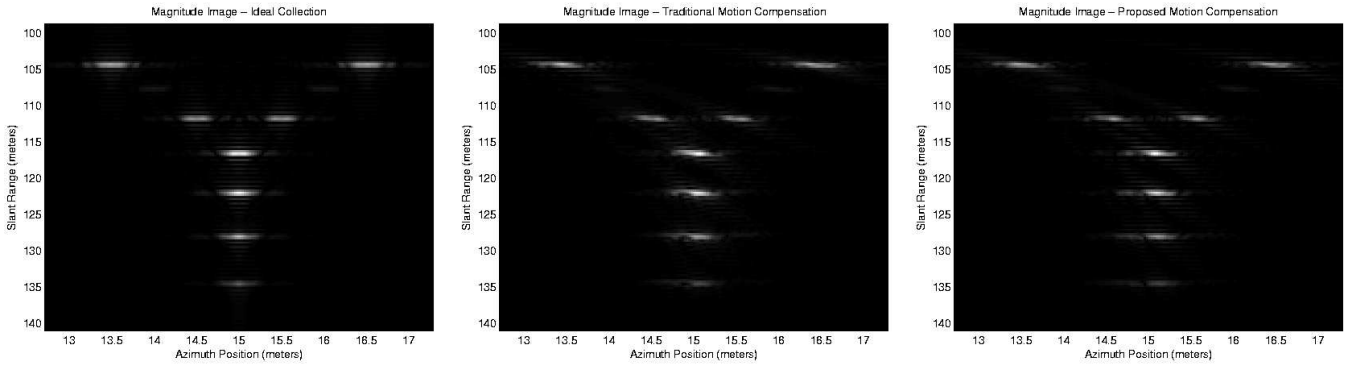

Fig. 7. A simulation of an array of point targets showing the motion compensation algorithms working on an array of point targets. The left shows an ideal collection without translational motion, the center shows the traditional motion correction algorithm, and the right shows the proposed motion correction. The non-ideal motion in this example is the same as in Fig. 6.

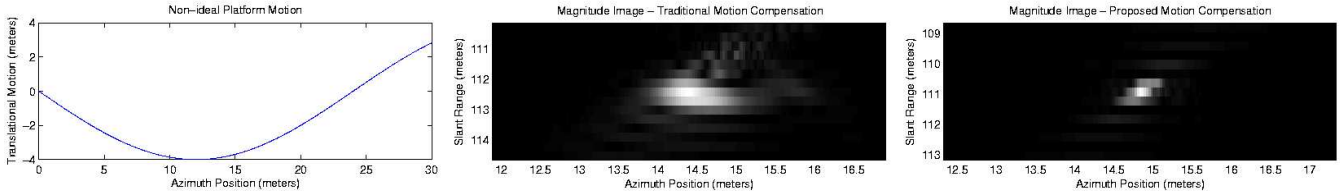

Fig. 8. Non-ideal translational motion greater than a single range bin (shown on the left) clearly demonstrates the utility of the new motion compensation algorithm as seen in this image of a point target. The center image shows the result of applying tradition motion compensation while the right image shows the proposed method.

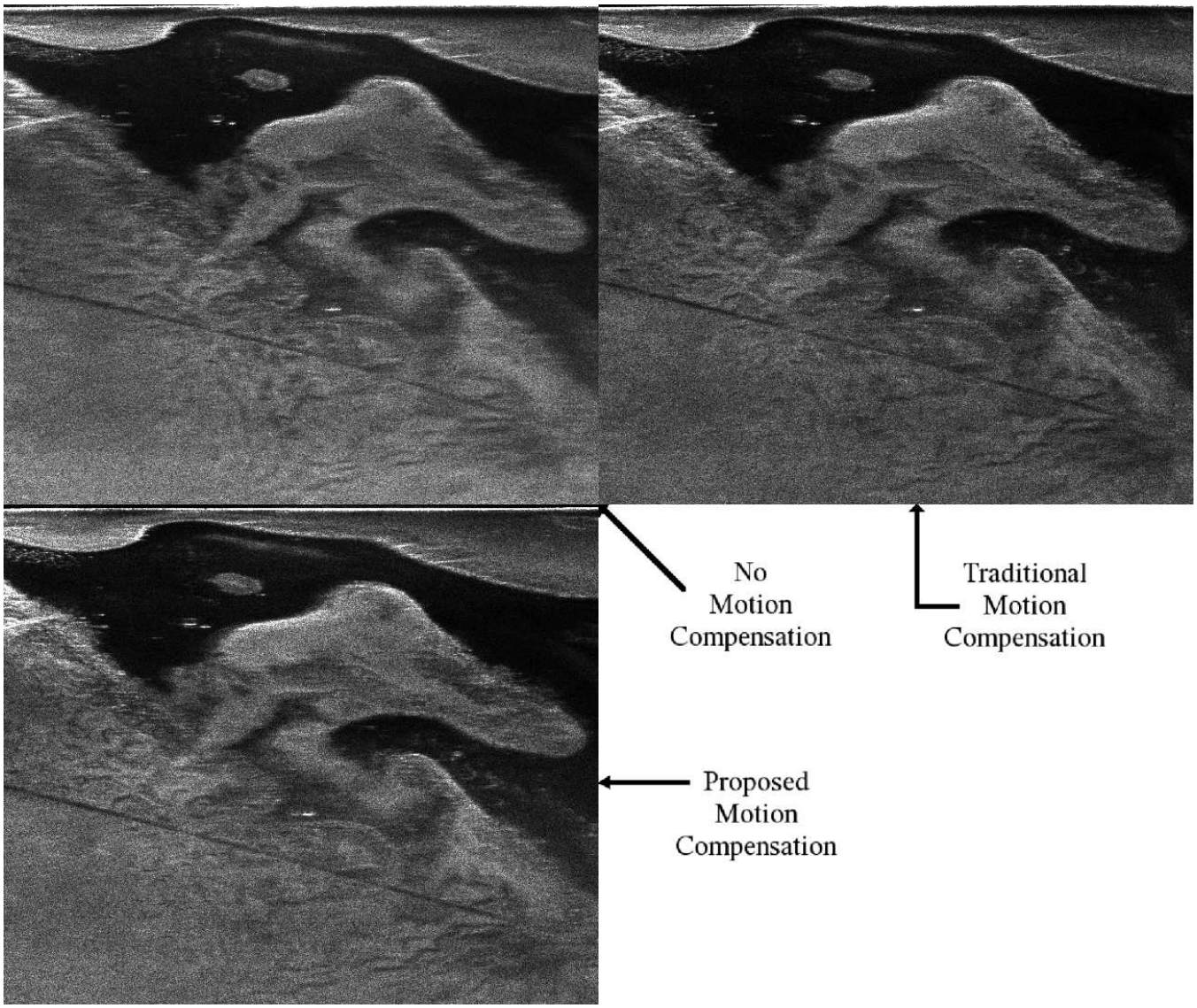

Fig. 9. Images created from NuSAR data, spanning an area of 778x654 meters, are presented with the results of traditional and proposed motion compensation algorithms. Of note is that the road crossing the lower half of the image is properly straightened when using the proposed motion compensation method.